



HAL
open science

4D characterisation of void nucleation, void growth and void coalescence using advanced void tracking algorithm on in situ X-ray tomographic data

M. A. Azman, C. Le Bourlot, A. King, D. Fabrègue, E Maire

► To cite this version:

M. A. Azman, C. Le Bourlot, A. King, D. Fabrègue, E Maire. 4D characterisation of void nucleation, void growth and void coalescence using advanced void tracking algorithm on in situ X-ray tomographic data. *Materials Today Communications*, 2022, 32, 10.1016/j.mtcomm.2022.103892 . hal-03763026

HAL Id: hal-03763026

<https://hal.science/hal-03763026>

Submitted on 5 Mar 2024

HAL is a multi-disciplinary open access archive for the deposit and dissemination of scientific research documents, whether they are published or not. The documents may come from teaching and research institutions in France or abroad, or from public or private research centers.

L'archive ouverte pluridisciplinaire **HAL**, est destinée au dépôt et à la diffusion de documents scientifiques de niveau recherche, publiés ou non, émanant des établissements d'enseignement et de recherche français ou étrangers, des laboratoires publics ou privés.

4D characterisation of void nucleation, void growth and void coalescence using advanced void tracking algorithm on *in situ* X-ray tomographic data

M.A. Azman^{a,b,*}, C. Le Bourlot^a, A. King^c, D. Fabrègue^a, E. Maire^a

^a INSA Lyon, MATEIS, University of Lyon, UMR 5510 CNRS, F-69621 Lyon, France

^b Universiti Putra Malaysia, 43400 Serdang, Selangor, Malaysia

^c SOLEIL synchrotron, L'Orme des Merisiers, BP 48, 91192 Gif-sur-Yvette, France

ARTICLE INFO

Keywords:

Ductile damage
Automatic cavity tracking
X-ray tomography
Void nucleation
Void growth
Void coalescence

ABSTRACT

An advanced tracking algorithm based upon 4D X-ray tomographic data was developed to enable a more robust and full field approach to ductile damage characterisation. By following each individual void, the three ductile damage mechanisms (void nucleation, void growth and void coalescence) could be separated and be studied in more detail, with enriched 4D information available for each of the three damage mechanisms. Here, a successful application of the developed tracking algorithm on a pure iron sample is presented. Two different notch geometries were chosen for the demonstration of analysis technique to further study the influence of triaxiality on ductile damage.

1. Introduction

Ductile damage in metals is a process involving three separate mechanisms, namely void nucleation [1,2], void growth [3,4] and void coalescence [5–9]. Void nucleation is usually associated with fracture of second phases such as particles and inclusions or interface decohesion [2,10–14]. However, in pure metals with no inclusions, void nucleation has also been observed at features such as grain boundaries [15–17], deformation-induced dislocation boundaries [18,19] and slip bands [20]. Stable growth continues until plasticity localises in the ligament between closely spaced cavities, leading to the coalescence mechanism. The build-up of void coalescences finally results in a macroscopic crack which eventually propagates across the entire material. The understanding and modelling of these three damage mechanisms have been enhanced over the years, as discussed in a number of review papers [7,8,21,22]. Damage inside a ductile material under tensile deformation has been shown to be a result of complex interaction of many different engineering and metallurgical variables [23].

Historically, microstructural post-mortem examination on samples using light or scanning electron microscopy has been the focus of experimental damage studies. More recently in the past three decades, X-ray tomography, especially synchrotron microtomography, has allowed *in situ* damage evolution during deformation to be analysed, both quantitatively and qualitatively [24,25]. The quantitative studies on the evolution of voids using X-ray tomography have focused on a mean-field statistical approach [24,26–31]. This approach is known to have

some intrinsic limitations. For example, nucleation and coalescence have an opposite effect on voids number and they can possibly occur at the same time. The volume porosity is also the result of a combination of void growth, newly nucleated voids and coalescence. Using X-ray tomography to quantify void growth in DP steels [32], Maire et al. showed that instead of increasing as expected for growing cavities, the mean radius calculated over the entire void population remained constant during the tensile test due to the small sized new nucleating voids. This mean radius is thus not suitable for the quantification of void growth. An acceptable approach to quantify void growth is by calculating the average of the N largest voids, but this is only suitable if these remain the same largest voids throughout deformation (which is probably untrue especially when coalescence occurs).

These limitations of the mean-field approach shows the strong need to separate the three different steps in order to obtain a clearer view of ductile damage. A previous study [29] has tried to separate the nucleation and void growth by using three-dimensional image analysis. In this method, further analysis of nucleation has been achieved but some limitation for growth and coalescence analysis still remains. A suitable method to achieve this goal, would be to follow the behaviour of each void. This can be conducted by connecting each voids individually at every time step of the process, thus enabling the separation of the three damage mechanisms and providing us deeper analysis. Manual tracking of cavities from one strain step to the next could lead to this goal but is extremely tedious. In the study of ductile damage, the number of

* Corresponding author at: Universiti Putra Malaysia, 43400 Serdang, Selangor, Malaysia.
E-mail address: amin.azman@upm.edu.my (M.A. Azman).

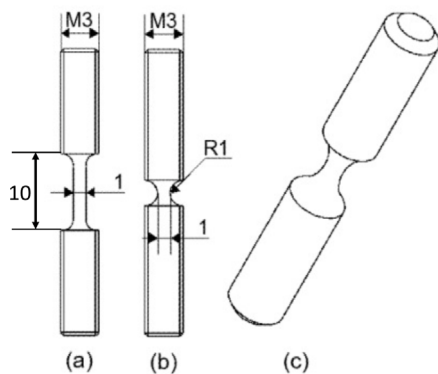


Fig. 1. Geometry of samples : (a) smooth specimen, (b) 1 mm radius notched specimen (c) 3D view.

objects to track is constantly changing due to the nucleation of new voids and the coalescence of previous voids. Tracking was manually performed by Landron but for a few number of selected cavities for one sample of dual phase steel (ferritic + martensite) [31]. Manually connecting all voids are however, not possible, as voids in certain materials can reach up to dozens of thousands in a scan. An automatic method is needed to achieve this. Toda et al. developed a tracking method of microstructural features for the purpose of visualisation of three-dimensional (3-D) strain map. Later on, Lecarme et al. has performed the tracking of voids in a TA6V alloy [33]. A similar automatic tracking algorithm based on these proofs of concept is further developed and presented in this study.

The goal of this paper is to show a successful application using this improved automatic cavity tracking algorithm for the characterising ductile damage. The damage evolution in a pure iron sample is captured by *in situ* synchrotron microtomography during tensile deformation of samples with geometries that induce different stress triaxialities. The tomographic data for these samples is then applied to the developed cavity tracking algorithm to follow each individual void. Once the voids are tracked, void nucleation, void growth and void coalescence can be studied separately and in more detail, with rich amount of 4D information. Position, time, shape and size of each of these cavities are now available for analysis. The outline of this paper is as follows: the X-ray microtomography technique is first introduced followed by an explanation of the tracking algorithm. The results obtained from the tracking algorithm are then presented, compared with the standard mean field analysis and discussed according to the three mechanisms: (i) void nucleation (ii) void growth, and (iii) void coalescence.

2. Experimental methods

2.1. Material

A stretched rod of very high purity (99.9%) iron provided by *Good-fellow* was investigated. The tomographic images of the investigated material shows that no initial cavities were detected in the material before the *in situ* tensile tests. However, it is possible that smaller voids are not being detected due to the limitation of the resolution as shown in the study by Landron et al. which shows a higher number of cavities detected at a higher resolution, compared to a lower resolution [34]. Axisymmetric samples of two different geometries were machined as shown in Fig. 1 previously used in [24]. Both the smooth and notched sample induces a different initial triaxiality which allows us to study the effect of this key parameter on damage.

2.2. Synchrotron X-ray microtomography during tensile tests

Synchrotron microtomography (SXCT) was carried out at the PSICHE Beamline of SOLEIL Synchrotron in France. Energy of 30 keV was used to acquire the radiographies. The voxel size from the acquired volume is $(0.87 \times 0.87 \times 0.87) \mu\text{m}^3$, with the minimum size of detected features (resolution) to be considered as voids being $2 \times 2 \times 2$ voxels ($5.27 \mu\text{m}^3$). The acquisition time for each scan was below 10 min. The samples were deformed using a dedicated tensile machine mounted on the rotation stage and described elsewhere [35]. The tensile tests were performed in an interrupted manner and the acquisitions were made in the centre of the specimen to follow the damage evolution of this region. The first tomography was acquired before traction as a reference acquisition, with subsequent acquisitions with increasing deformation steps until fracture.

The raw volumes obtained from the reconstruction of the tomography scans were then median filtered and thresholded. This procedure allows the separation of voids from the material. Each void was then subsequently labelled and all the quantitative information, as well as qualitative representations of each void, were extracted. Both the tomograms processing and cavities extraction were performed with the ImageJ software package [36]. The minimal section represents the Z section of the material which has the smallest area. To determine this, the area of every image slice of the materials (without voids) as a function of Z was first calculated, as shown in Fig. 3. This graph was then fitted to a parabolic curve to avoid the interference of any noise and quality of machining. The Z slice with the lowest value on the fitted curve was then easily identified. The actual area of that Z slice represents the minimal section.

The macroscopic average value of true strain and true stress in the minimal section were determined using the following equations, as further described by Landron et al. [24]:

$$\sigma_{zz} = \frac{F}{S} \quad (1)$$

$$\epsilon_{zz} = \ln\left(\frac{S_0}{S}\right) \quad (2)$$

where S , S_0 represent the minimal area, and initial minimal area respectively.

The effect of sample geometry on stress triaxiality and its evolution during straining were determined from the experiments. The curvature radius R_{notch} and the radius of the minimal section, $R_{section}$ were measured in order to determine the average stress triaxiality T in the centre of the minimum cross-section using the Bridgman formula [37] as reassessed by Wierzbicki and Bai [38] described by Landron et al. [25]:

$$T = \frac{1}{3} + \sqrt{2} \ln\left(1 + \frac{R_{Section}}{2R_{Notch}}\right) \quad (3)$$

The use of these equations were validated with finite elements (FE) simulations which shows the results of the simulations are in good agreement with the true strain calculated from Eq. (2) and with the stress triaxiality calculated from Eq. (3) [24] (see Fig. 2).

2.3. Automatic tracking algorithm

Once the images have been processed to identify and extract the parameters (coordinates of the centre of mass, volume, shape, etc.) of each cavity, this list of parameters can then be analysed using the automatic tracking method. This developed tracking algorithm, written in the python language, is largely based on the previous tracking algorithm used in [33]. The basic principle of this method is to associate all individual voids across different time steps as shown in Fig. 2. This is commonly known as Particle Image Velocimetry and have been used in different domains such as in biology [39], earth science [40], etc. Graph-based approaches have been commonly adopted to solve these data association problems. In this framework, each feature is defined

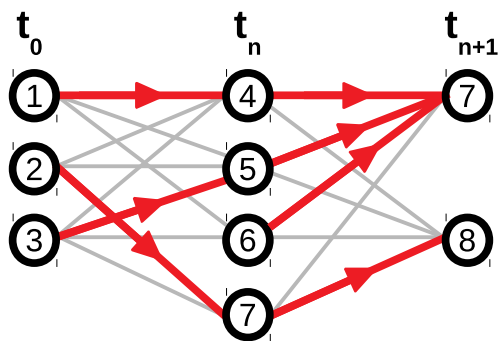


Fig. 2. Schematic example of the tracking algorithm. In grey are the connection of probability between a node in one time step and all the nodes the following time step. In red, is the connection with the highest probability is chosen as the final track.

as a node in the graph. Every node of a single timestep (t) is connected (with edges) to every nodes in next time step ($t + 1$) until the end. Thus, every edges is an associated probability (or a weight). This is the probability that these two nodes are connected. This probability graph is used as input to a shortest path algorithm (here a Dijkstra algorithm [41]) to extract all the tracks.

The probability calculation has to take the specificity of the studied system into account. In our case of ductile damage analysis, it has consider that (i) voids can nucleate at any moment, (ii) voids evolve in size and shape with deformation, and (iii) voids can coalesce into one. Moreover, voids do not move during the experiment, except due to the movement of the sample and the strain flow of the matter during the *in situ* tensile test. Manual rigid body and strain-flow correction are applied to the data to correct drift of the sample during the *in situ* acquisitions to ensure the same voids remains as close as possible to their original position. After applying correction, the criteria then used to calculate the probabilities, based on the mentioned specificities of ductile damage analysis above, are:

- **Distance:** the distance between features, if drift has been corrected, is the first and most relevant criteria
- **Size:** the evolution of the volume should follow some trends. A void volume can decrease a bit but not drastically. Fluctuation from segmentation has to be considered. When the followed features are inclusions, the volume should not change, except due to threshold approximations.
- **Shape, inertia, orientation, sphericity:** different characteristics extracted during the process can possibly be used to further refine the calculation of probability.

Some of these criteria are simple to compute, such as point-to-point distances, but others are more time consuming such as surface-to-surface distances. As the number of voids can reach up to dozen of thousands in a sample at a single time step, each acquisition adds thousands of nodes in the system and therefore millions of edges in the probability graph. This can be a very time-consuming process, especially in taking account of the physical aspects of the voids. To reduce the time calculation process, a preliminary “first rough probability” filtering process is introduced to quickly eliminate most of the improbable connections, prior to the final and more accurate calculation. This drastically reduces the time and resources needed for calculation.

This two-step approach is detailed below. For the algorithm complexity evaluation, the complexity is defined as $O(nt)$, n being the number of nodes for an acquisition, and t the number of acquisitions:

- Step 1: A first rough evaluation of the probability graph is computed as a set of interaction matrix using bounding box distances: null if the bounding boxes overlap, or otherwise if the euclidean distance exists between the bounding boxes. The implementation is fast and easily vectorised. A threshold cancellation of most of the edges because of their very low probability. The complexity of an interaction matrix evaluation is $O(n^2)$, the overall complexity is therefore $O(tn^2)$ and the number of edges tn^2 . The threshold allows to keep only few probable edges per node therefore around tn edges only.
- Step 2: The remaining probable nodes are evaluated individually with higher precision but in more complex algorithms. The remaining edges values are stored in a sparse matrix.¹ The stored data for a sparse matrix would be around $3 \times$ the number of computed edges, instead of $t^2 n^2$ with only tn^2 non-null edges for a classical matrix. As voids can go undetected during deformation if it leaves the field of view, an additional node (called “black hole”) is added to allow the tracks to stop at any moment. All the tracks are set to end at this “black hole”. The final interaction (sparse) matrix is used with a ‘Dijkstra Shortest Path Algorithm’² between all nodes and the “black hole”.

The extracted graph containing all the tracks is similar to a family tree. The highest ancestors: nodes without parent, are nucleation. The children : nodes with 2 or more parents are the result of coalescences. Nodes with only one parent are just due to the evolution of the same

¹ Implemented in the code as a scipy.sparse matrix: <https://docs.scipy.org/doc/scipy/reference/sparse.html>.

² <https://docs.scipy.org/doc/scipy/reference/generated/scipy.sparse.csgraph.dijkstra.html>.

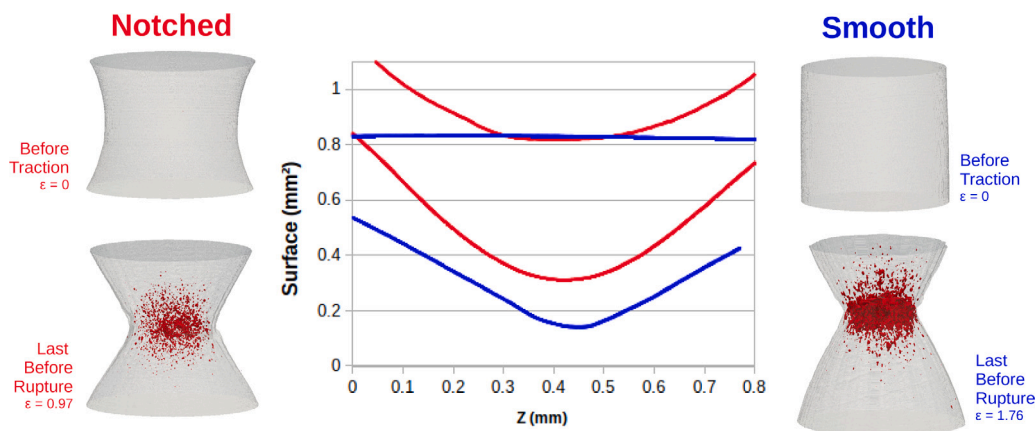


Fig. 3. 3D visualisation and the calculated cross section area as a function of Z of both samples of first acquisition before tracking and last acquisition before rupture.

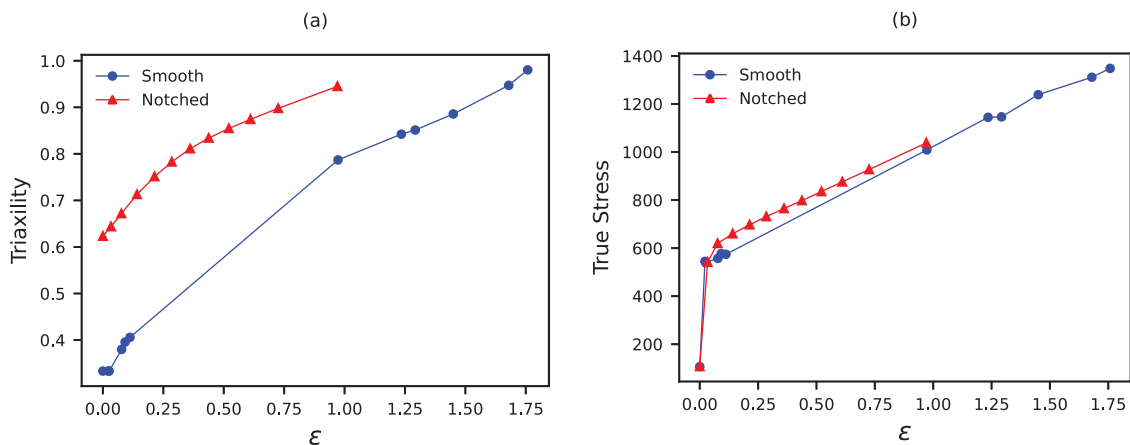


Fig. 4. Evolution of (a) true stress and (b) triaxiality calculated in the pure iron sample for both geometry notch samples as a function of true strain.

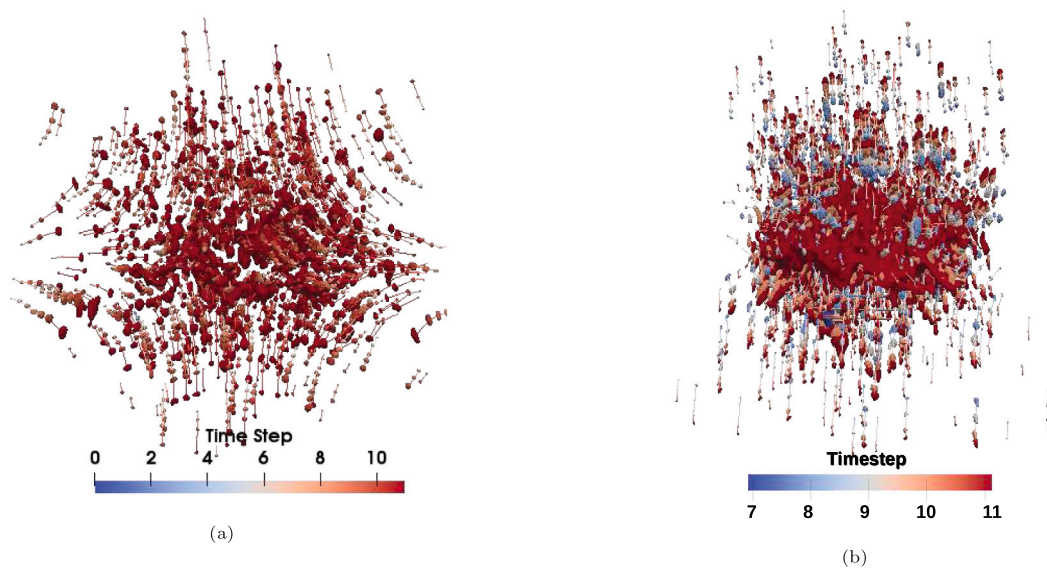


Fig. 5. Tracking of voids in both (a) notched and (b) smooth iron sample.

void during the *in situ* tensile test, therefore “pure void growth”. A node which points directly towards the “black hole” is a track termination: because the track continues outside the field of view or because this is the last acquisition step. A node with no parent and no child, is considered a non-tracked feature and is most probably an artefact from segmentation (noise, part of reconstruction rings, etc...).

3. Results and discussion

3.1. Macroscopic measurements

Fig. 3 shows the 3D perspectives of damage in both the notched and smooth sample of the pure iron material at the beginning (first acquisition before traction) and at the end (last acquisition before rupture). The calculation of the cross-sectional area as a function of Z from the tomographic data is also presented. While both have the same middle cross-sectional area at the beginning ($D = 1 \text{ mm}$, $S = 0.79 \text{ mm}^2$), the cross section area of the final acquisition is lower for the smooth sample compared to the notched sample indicating higher ductility.

Macroscopic mechanical measurements of the *in situ* tensile test are shown on Fig. 4. Fig. 4(a) shows the triaxialities calculated in notched and smooth sample. The initial triaxiality of notched sample is around

0.62, while for the smooth sample it is 0.33. This is in agreement with the theoretical values, with the notched sample being slightly below the expectation, probably due to the quality of machining. Both curves show a rather linear relationship between triaxiality and true strain. Fig. 4(b) shows the tensile true stress of the samples studied as a function of the local tensile true strain. These curves show the mechanical behaviour of the pure iron sample for both geometries. They are in agreement with expectations as triaxiality increases the ‘apparent’ strength of a material. The notched sample, which induces a higher initial triaxiality, has a slightly higher yield stress value compared to the smooth sample, also observed in other materials [32]. This well-known ‘apparent hardening’ effect is due to the building of stresses in the transverse direction of the notched samples. As expected, the macroscopic ductility of the notched samples is also reduced.

3.2. Damage characterisation using automatic cavity tracking

The tracking algorithm was applied to the tomographic data. Fig. 5 shows the output of the tracking. Each individual void is being tracked from the moment it nucleates until the final timestep. Different colours represent a different time step. Only the tracked voids in the central area of the tensile specimen were selected for damage quantification. It can be assumed that this central sub-region undergoes the highest

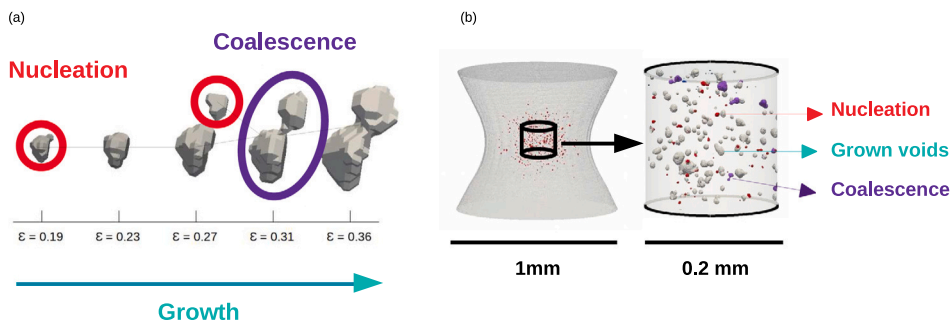


Fig. 6. 3-D views of (a) a track across different time steps, and (b) sample volume and voids in a single step acquisition voids obtained by tomography. The central cylindrical sub region is chosen for ductile damage characterisation. With tracking, the voids can be separated into the 3 damage mechanism of nucleation, growth and coalescence.

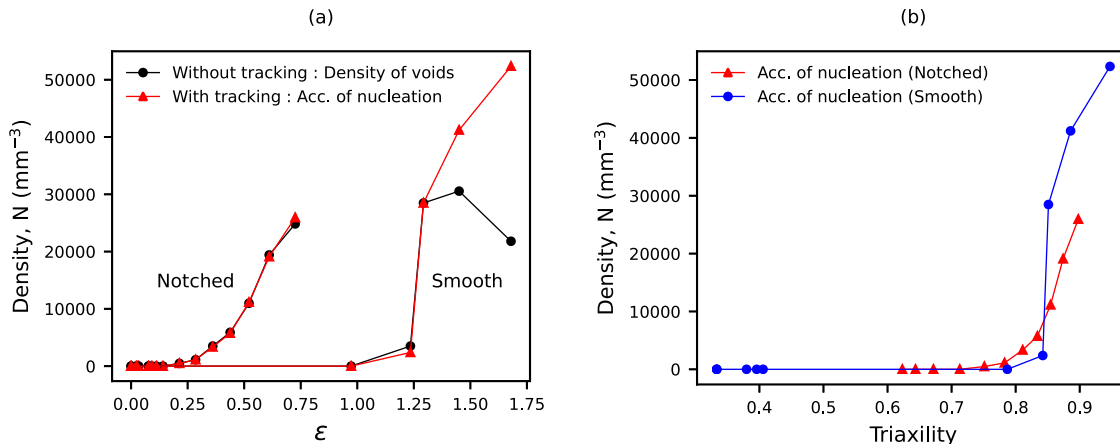


Fig. 7. Comparison of accumulation density of nucleation (from tracking) and density of voids (without tracking) with the in both samples as a function of (a) true strain and (b) triaxiality. The density of voids is traditionally used to characterise nucleation.

stress triaxiality state and the highest strain during the tensile test. This sub-region was chosen to be a cylindrical volume of diameter and length equal to 200 μm , as indicated in Fig. 6. The size was chosen to be sufficiently large for the elementary volume to be representative but also sufficiently small for the strain and triaxiality to be spatially close to constant inside this sub-volume. FE simulations [42] show that the spatial fluctuation of the strain over an almost similar sub-volume in the notched sample was less than 4%, hence assuming that it is constant is not far from reality.

Fig. 6(a) shows an example of a single track using the tracking algorithm. Fig. 6(b) shows the voids of a single acquisition being separated into nucleation, growth and coalescence. Non tracked features, or features which are chosen to be part of any track will be discarded from any analysis. These features are usually residues of un-removed ring artefacts.

The quantitative characterisations of void nucleation, growth and coalescence are presented separately in the following sub-sections.

3.3. Void nucleation

Fig. 7(a) shows the quantification of nucleation with deformation. It is observed that the nucleation starts at lower strain values for the notched sample, consistent with previous studies in [31,43]. These nucleation accumulation density values are also compared with the density of voids, which is the classical method to quantify nucleation (in the mean field approach without tracking). Both void densities shows good agreement with the accumulated density of nucleation up until large coalescence events. After strain value of around 1.3 in the smooth sample, a huge difference between the density of voids and the accumulated number of nucleation can be observed. Tracking then

clearly helps us here to continue quantifying nucleation long after coalescence has occurred, showing a more precise number of voids. Noise or un-removed disconnected ring artefacts which can be mistakenly counted as voids and increase the density of voids, can also be removed as “non-tracked features” as can be seen at $\epsilon = 1.25$ for the smooth sample. This is, however, a minor mis-quantification of nucleation compared to the effect of coalescence. The density of nucleated voids measured using tracking is plotted again as a function of triaxiality in Fig. 7(b). It can be observed that the increase of nucleation starts at almost the same triaxiality value and that the density of nucleated voids as a function of triaxiality is strikingly similar in both samples. This shows that stress triaxiality is the main driving force for the nucleation of voids. The extraction of all the nucleated voids allows characteristics of nucleation to be studied. The nucleated voids in the notched and smooth sample have an average sphericity of 0.86 and 0.88 respectively. The sphericity refers to ratio of the surface area of a sphere with the same volume of the feature to the actual surface area of the feature [44], with the sphericity value varying between 0 and 1 (the value of 1 indicates a perfect sphere). These values of sphericity show that the nucleated voids are rather spherical in shape. This is consistent with the hypothesis that pure metals nucleate spherical voids rather than prolate microcracks as it is the case for inclusion fracture in engineering alloys [45].

3.4. Void growth

The void growth volume of all individual voids for the notched sample is shown in Fig. 8 (black), together with the evolution of the average size of the Nth largest voids (colour). The graphs show that the voids nucleates at different strain values and that after nucleation, their size increases with deformation. The evolution of single large

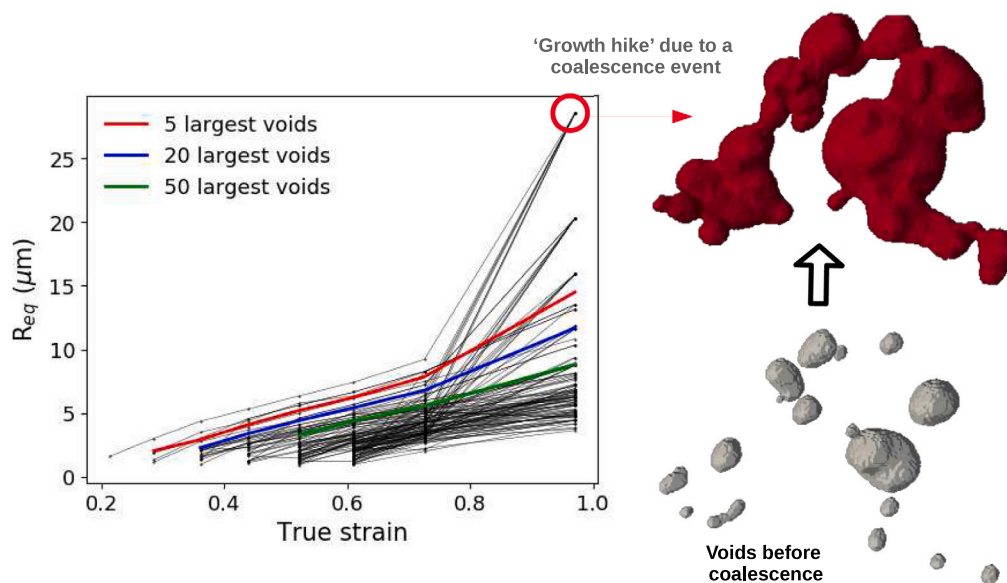


Fig. 8. Evolution of volume growth (R_{eq}) of the individual voids with coalescence events of the notched sample.

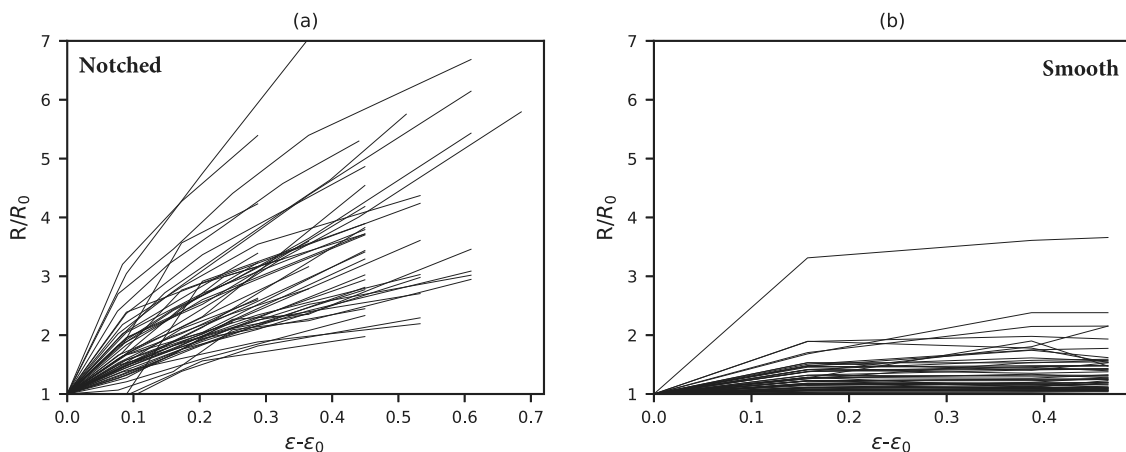


Fig. 9. Evolution of volume growth (R/R_0) of the individual voids without coalescence as a function of normalised strain in (a) notched and (b) smooth sample. The scale is similar, for comparison. Only long tracks have been kept, for readability (more than 4 consecutive steps).

pores from the tracking is similar to those of the average of 5 and 20 largest cavities (mean-field approach) as discovered by [24]. However this is only true at low strain. Growth hikes can be observed especially at higher strain, the largest single pores merging towards this growth hikes. This confirms again the assumption that acceleration in growth especially at the end is due to coalescence events of the largest voids. Therefore, it highlights a small limitation in the classical approach of studying the N largest voids, in which the studied N voids no longer remains the same when there is coalescence of voids.

Using the information obtained from track, another way to study the growth process and compare between the voids is to focus only the growth before the coalescence process occurs and normalise both the volume and true strain. Fig. 9 shows volume evolution of every cavity normalised by its volume at nucleation (R/R_0), as a function of its effective growing strain ($Strain - Strain\ at\ nucleation$). Significant differences in the growth kinetics are observed for the different cavities. The voids in the notched samples appear to grow faster compared to those in the smooth sample, showing that increasing stress triaxiality leads to an increase of the rate of porosity growth, as expected from Rice and Tracey [46]. However this does not explain the heterogeneity of void growth which is probably due to the local microstructure and

grain orientations. These heterogeneities are visible on both sample, and could even imply negative voids growth rate.

3.5. Void coalescence

With the tracking algorithm, all the coalescence events can be automatically and rather easily separated, analysed and visualised. This is a major improvement compared to our previous study where this analysis had to be made manually and was so tedious that it was not reproduced on many samples. Fig. 10 is a 3D visualisation of coalescence events extracted in the sub-volume of the notched sample with 2 zoomed-in examples with their coalescing voids. Each colour represents the time step in which the coalescence void occurs. Fig. 8 shows another example of a coalescence event in the notched sample. This coalescence event is a result of 17 smaller voids merging. The ability of tracking in capturing this large coalescence event shows the precision of the algorithm.

In the literature, it has been observed that coalescence events are distinguished depending on the orientation of the tensile axis compared to the axis between the centre of mass of the two coalescing cavities : intervoid necking (90°), intervoid shearing (45°), and necklace coalescence (0°). Fig. 11 shows the number of coalescence as a function of this

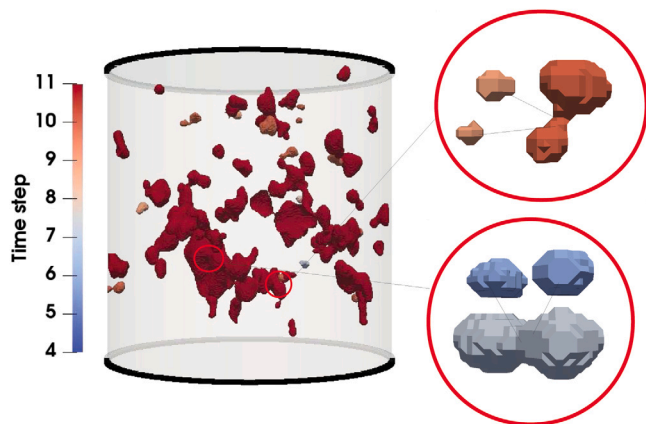


Fig. 10. Coalescence of voids in the studied sub-volume extracted by the tracking algorithm.

orientation in both the notched and smooth sample. For the notched sample, the majority of coalescence events are between voids of around 75 degrees apart, while for the smooth sample, it is around 45 degrees. This shows that the stress triaxiality has an effect on the orientation of coalescence.

4. Conclusion

The evolution of damage during tensile loading of a pure iron material was investigated *in situ* by synchrotron micro-tomography and then analysed using a newly-developed automatic tracking algorithm. Using the automatic tracking algorithm on tomographic data has enable a more full-field approach for ductile damage characterisation. This new way of obtaining the quantitative results has been shown to be more robust than the standard statistical mean-field approach. The evolution of each individual void can be followed, allowing the three damage mechanisms to be studied separately, with enriched 4D information available for each of the damage mechanism:

- **Void nucleation:** the quantification of nucleation can now be performed in a more accurate manner, especially with the presence of coalescence. The characteristics of all nucleated voids can also now be obtained (size, shape, position, etc.).
- **Void growth:** the growth evolution of each of these individual nucleated voids can be followed with deformation. This allows to

study the heterogeneity of the evolution of voids. The evolution can be studied up to a coalescence event for pure void growth analysis.

- **Void coalescence:** coalescence events can be detected automatically, allowing for a much easier study of the characteristics of the coalescing voids (size, shape, position, distance between coalescing voids, etc.).

The effect of triaxiality induced by the sample geometry on ductile damage has also been presented in this study. The notched sample with a higher initial triaxiality, has shown to have a lower nucleation strain rate and a higher void growth rate. The triaxiality also seems to have an effect the orientation between coalescing voids.

The tracking algorithm will open up a lot of different possibilities in the field of study of ductile damage using tomographic data, such as:

- studying the evolution of different population of voids,
- comparing voids from different nucleation sites such as nucleation from brittle particles fracture or interface decohesion,
- comparing the evolution of initial pre-existing voids with nucleated voids during deformation.

CRediT authorship contribution statement

M.A. Azman: Investigation, Writing – original draft. **C. Le Bourlot:** Investigation, Writing – original draft, Writing – review & editing, Software, Supervision. **A. King:** Resources. **D. Fabrègue:** Writing – review & editing. **E. Maire:** Funding acquisition, Supervision, Writing – review & editing.

Declaration of competing interest

The authors declare that they have no known competing financial interests or personal relationships that could have appeared to influence the work reported in this paper.

Data availability statement

The raw/processed data required to reproduce these findings cannot be shared at this time as the data also forms part of an ongoing study.

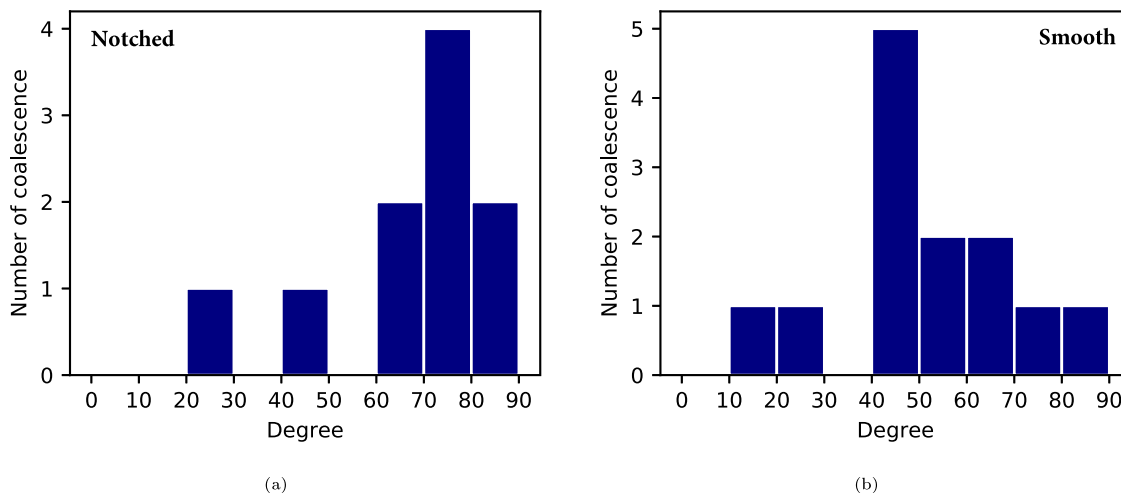


Fig. 11. The orientation angle between 2 coalescing voids of the (a) notched sample and (b) smooth sample.

Acknowledgements

The authors would like to thank SOLEIL for the provision of synchrotron radiation facilities at the PSICHE beamline, and Marta Gallo, Shoya Aota and Lucile Magnier for the X-ray tomography experiments. The authors acknowledge the Ministry of Education of Malaysia and Universiti Putra Malaysia for the PhD scholarship provided to M.A. Azman.

References

- [1] S.H. Goods, L.M. Brown, Overview no. 1. The nucleation of cavities by plastic deformation, *Acta Metall.* 27 (1) (1979) 1–15.
- [2] A.S. Argon, R. Safoglu, Cavity formation from inclusions in ductile fracture, vol. 6, (April) 1975.
- [3] K.E. Puttick, Ductile fracture in metals, *Philos. Mag. J. Theor. Exper. Appl. Phys.* 4 (44) (1959) 964–969.
- [4] S. Floreen, H. Hayden, Some observations of void growth during the tensile deformation of a high strength steel, *Scr. Metall.* 4 (2) (1970) 87–94.
- [5] A.W. Thompson, Modeling of local strains in ductile fracture, *Metall. Trans. A* 18 (11) (1987) 1877–1886.
- [6] I.G. Park, A.W. Thompson, Ductile fracture in spheroidized 1520 steel, *Acta Metall.* 36 (7) (1988) 1653–1664.
- [7] A. Pineau, A.A. Benzerga, T. Pardoen, Failure of metals I: Brittle and ductile fracture, *Acta Mater.* 107 (2016) 424–483.
- [8] A.A. Benzerga, J.-b. Leblond, Ductile fracture by void growth to coalescence, in: *Advances in Applied Mechanics - Volume 44*, Vol. 44, Elsevier Inc., 2010, pp. 169–305.
- [9] T. Petit, J. Besson, C. Ritter, K. Colas, L. Helfen, T.F. Morgener, Effect of hardening on toughness captured by stress-based damage nucleation in 6061 aluminum alloy, *Acta Mater.* 180 (2019) 349–365.
- [10] K. Tanaka, T. Mori, T. Nakamura, Cavity formation at the interface of a spherical inclusion in a plastically deformed matrix, *Phil. Mag.* 21 (170) (1970) 267–279.
- [11] N. Kanetake, M. Nomura, T. Choh, Continuous observation of microstructural degradation during tensile loading of particle reinforced aluminium matrix composites, *Mater. Sci. Technol. (United Kingdom)* 11 (12) (1995) 1246–1252.
- [12] D. Seo, H. Toda, M. Kobayashi, K. Uesugi, A. Takeuchi, Y. Suzuki, In situ observation of void nucleation and growth in a steel using X-ray tomography, *ISIJ Int.* 55 (7) (2015) 1474–1482.
- [13] Y. Shen, T.F. Morgener, J. Garnier, L. Allais, L. Helfen, J. Crépin, D. Rozumek, Quantitative anisotropic damage mechanism in a forged aluminum alloy studied by synchrotron tomography and finite element simulations, *Adv. Mater. Sci. Eng.* 2019 (2019).
- [14] C.F. Kusche, F. Pütz, S. Münstermann, T. Al-Samman, S. Korte-Kerzel, On the effect of strain and triaxiality on void evolution in a heterogeneous microstructure – a statistical and single void study of damage in DP800 steel, *Mater. Sci. Eng. A* 799 (September 2020) (2020) 140332.
- [15] E.M. Bringa, S. Traiviratana, M.A. Meyers, Void initiation in fcc metals: Effect of loading orientation and nanocrystalline effects, *Acta Mater.* 58 (13) (2010) 4458–4477.
- [16] O. Rezvanian, M.A. Zikry, A.M. Rajendran, Statistically stored, geometrically necessary and grain boundary dislocation densities: Microstructural representation and modelling, *Proc. R. Soc. A: Math. Phys. Eng. Sci.* 463 (2087) (2007) 2833–2853.
- [17] T.R. Bieler, M.A. Crimp, Y. Yang, L. Wang, P. Eisenlohr, D.E. Mason, W. Liu, G.E. Ice, Strain heterogeneity and damage nucleation at grain boundaries during monotonic deformation in commercial purity titanium, *JOM* 61 (12) (2009) 45–52.
- [18] P. Noell, J. Carroll, K. Hattar, B. Clark, B. Boyce, Do voids nucleate at grain boundaries during ductile rupture? *Acta Mater.* 137 (2017) 103–114.
- [19] N. Hansen, R.F. Mehl, New discoveries in deformed metals, *Metall. Mater. Trans. A: Phys. Metall. Mater. Sci.* 32 (12) (2001) 2917–2935.
- [20] O. Furukimi, C. Kiattisaksri, Y. Takeda, M. Aramaki, S. Oue, S. Munetoh, M. Tanaka, Void nucleation behavior of single-crystal high-purity iron specimens subjected to tensile deformation, *Mater. Sci. Eng. A* 701 (March) (2017) 221–225.
- [21] P.J. Noell, J.D. Carroll, B.L. Boyce, The mechanisms of ductile rupture, *Acta Mater.* 161 (2018) 83–98.
- [22] A. Pineau, T. Pardoen, 2.06 - Failure of metals, *Compr. Struct. Integr.* 2 (2007) 684–797.
- [23] A. Das, Stress/strain induced void? *Arch. Comput. Methods Eng.* 28 (3) (2021) 1795–1852.
- [24] C. Landron, E. Maire, O. Bouaziz, J. Adrien, L. Lecarme, A. Bareggi, Validation of void growth models using X-ray microtomography characterization of damage in dual phase steels, *Acta Mater.* 59 (20) (2011) 7564–7573.
- [25] C. Landron, O. Bouaziz, E. Maire, J. Adrien, Experimental investigation of void coalescence in a dual phase steel using X-ray tomography, *Acta Mater.* 61 (18) (2013) 6821–6829.
- [26] E. Maire, S. Zhou, J. Adrien, M. Dimichiel, Damage quantification in aluminium alloys using in situ tensile tests in X-ray tomography, *Eng. Fract. Mech.* 78 (15) (2011) 2679–2690.
- [27] N. Pathak, C. Butcher, J. Adrien, E. Maire, M. Worswick, Micromechanical modelling of edge failure in 800 MPa advanced high strength steels, *J. Mech. Phys. Solids* 137 (2020).
- [28] S. Thuillier, E. Maire, M. Brunet, Ductile damage in aluminium alloy thin sheets: Correlation between micro-tomography observations and mechanical modeling, *Mater. Sci. Eng. A* 558 (2012) 217–225.
- [29] G. Requena, E. Maire, C. Leguen, S. Thuillier, Separation of nucleation and growth of voids during tensile deformation of a dual phase steel using synchrotron microtomography, *Mater. Sci. Eng. A* 589 (2014) 242–251.
- [30] T. Balan, X. Lemoine, E. Maire, A.M. Habraken, Implementation of a damage evolution law for dual-phase steels in guron-type models, *Mater. Des.* 88 (2015) 1213–1222.
- [31] C. Landron, O. Bouaziz, E. Maire, J. Adrien, Characterization and modeling of void nucleation by interface decohesion in dual phase steels, *Scr. Mater.* 63 (10) (2010) 973–976.
- [32] E. Maire, O. Bouaziz, M. Di Michiel, C. Verdu, Initiation and growth of damage in a dual-phase steel observed by X-ray microtomography, *Acta Mater.* 56 (18) (2008) 4954–4964.
- [33] L. Lecarme, E. Maire, A. Kumar K.c., C. De Vleeschouwer, L. Jacques, A. Simar, T. Pardoen, Heterogenous void growth revealed by in situ 3-D X-ray microtomography using automatic cavity tracking, *Acta Mater.* 63 (2014) 130–139.
- [34] C. Landron, E. Maire, J. Adrien, O. Bouaziz, M. Di Michiel, P. Cloetens, H. Suhonen, Resolution effect on the study of ductile damage using synchrotron X-ray tomography, *Nucl. Instrum. Methods Phys. Res. B* 284 (2012) 15–18.
- [35] J.Y. Buffiere, E. Maire, J. Adrien, J.P. Masse, E. Boller, In situ experiments with X ray tomography: an attractive tool for experimental mechanics, *Exp. Mech.* 50 (3) (2010) 289–305.
- [36] J. Schindelin, I. Arganda-Carreras, E. Frise, V. Kaynig, M. Longair, T. Pietzsch, S. Preibisch, C. Rueden, S. Saalfeld, B. Schmid, J.Y. Tinevez, D.J. White, V. Hartenstein, K. Eliceiri, P. Tomancak, A. Cardona, Fiji: AN open-source platform for biological-image analysis, *Nature Methods* 9 (7) (2012) 676–682.
- [37] P.W. Bridgman, Effects of high hydrostatic pressure on the plastic properties of metals, *Rev. Modern Phys.* (1945).
- [38] Y. Bai, X. Teng, T. Wierzbicki, On the application of stress triaxiality formula for plane strain fracture testing, *J. Eng. Mater. Technol.* 131 (2) (2009) 021002.
- [39] M. F., J.C. Winterwerp, An experimental study into the evolution of the size distribution of kaolinite flocs, *Proc. Mar. Sci.* 8 (2007) 55–73.
- [40] I. Grant, Particle image velocimetry: A review, *Proc. Inst. Mech. Eng. Part C: J. Mech. Eng. Sci.* 211 (1) (1997) 55–76.
- [41] E.W. Dijkstra, A note on two problems in connexion with graphs, *Numer. Math.* 1 (1) (1959) 269–271.
- [42] E. Maire, T. Morgener, C. Landron, J. Adrien, L. Helfen, Bulk evaluation of ductile damage development using high resolution tomography and laminography, *Comptes Rendus Phys.* 13 (3) (2012) 328–336.
- [43] G. Testa, N. Bonora, A. Ruggiero, G. Iannitti, D. Gentile, Stress triaxiality effect on void nucleation in ductile metals, *Fatigue Fract. Eng. Mater. Struct.* 43 (7) (2020) 1473–1486.
- [44] G. Ziółkowski, E. Chlebus, P. Szymczyk, J. Kurzac, Application of X-ray CT method for discontinuity and porosity detection in 316l stainless steel parts produced with SLM technology, *Arch. Civ. Mech. Eng.* 14 (4) (2014) 608–614.
- [45] N. Dang, L. Liu, J. Adrien, S. Cazottes, W. Xiao, C. Ma, L. Zhou, E. Maire, Materials science & engineering a crack nucleation and growth in α/β titanium alloy with lamellar microstructure under uniaxial tension : 3D X-ray tomography analysis, *Mater. Sci. Eng. A* 747 (January) (2019) 154–160.
- [46] J.R. Rice, D.M. Tracey, On the ductile enlargement of voids in triaxial stress fields*, *J. Mech. Phys. Solids* 17 (3) (1969) 201–217.